Title

New Techniques in MR Imaging of the Ankle and Foot

Journal

Magnetic Resonance Imaging Clinics of North America, 25(1)

ISSN

1064-9689

Authors

Bae, Won C
Ruangchaijatuporn, Thumanoon
Chung, Christine B

Publication Date

2017-02-01

DOI

10.1016/j.mric.2016.08.009

Peer reviewed

HHS Public Access

Author manuscript

Magn Reson Imaging Clin N Am. Author manuscript; available in PMC 2018 February 01.

Published in final edited form as:

Magn Reson Imaging Clin N Am. 2017 February ; 25(1): 211–225. doi:10.1016/j.mric.2016.08.009.

New Techniques in MR Imaging of the Ankle and Foot

Won C. Bae, Ph.D.[1,2] **[Assistant Professor]**, **Thumanoon Ruangchaijatuporn, M.D.**[3] **[Faculty of Medicine]**, and **Christine B. Chung, M.D.**[1,2] **[Professor]**

Won C. Bae: wbae@ucsd.edu; Thumanoon Ruangchaijatuporn: thumanoon.rua@outlook.com; Christine B. Chung: cbchung@ucsd.edu

[1]Radiology Service, Veterans Affairs San Diego Healthcare System, 3350 La Jolla Village Drive, MC 114, San Diego, CA 92161

[2]Department of Radiology, University of California, San Diego, UCSD MSK Imaging Research Lab, 9427 Health Sciences Drive, La Jolla, CA 92093-0997

[3]Department of Diagnostic and Therapeutic Radiology, Faculty of Medicine Ramathibodi Hospital, Mahidol University, 270 Rama VI Road, Rachathewi, Bangkok, Thailand 10400

Synopsis

Foot and ankle disorders are commonplace in everyday clinical practice. Magnetic resonance imaging (MRI) is frequently required for accurate diagnosis given the broad spectrum of pathology and complexity of foot and ankle anatomy. While conventional MRI plays a significant role for diagnosis, contemporary management increasingly relies upon advanced imaging for monitoring therapeutic response. Subsequently, there is an expanding need for identification of biomarkers for musculoskeletal tissues such as cartilage, tendon, bone and nerves. Advanced imaging techniques capable of imaging these tissue substrates will be increasingly utilized in routine clinical practice. Radiologists should therefore become familiar with these innovative MR techniques. Many such techniques are already widely used in other organ systems, such as isotropic 3D imaging acquisitions, diffusion weighted imaging, and kinematic imaging. Other techniques have until recently been limited to the research realm, and include MR neurography, ultrashort TE MRI and quantitative MRI.

Keywords

Magnetic Resonance Imaging; 3D Isotropic MRI; MR Neurography; Diffusion Weighted Imaging; Sodium MR; Ultrashort TE; Quantitative MRI; Ankle

Introduction

Pathology of the foot and ankle, both in the setting of acute diagnosis and follow up of lesions, are an important part of any musculoskeletal imaging practice. The incidence of foot

The authors have nothing to disclose

and ankle injuries has been reported to represent as high as 10% of all trauma cases [1]. Costs related to diabetic foot ulcer care are greater than $1 billion annually and rising, with neuropathy and infection accounting for 90% of related admissions [2]. While only 3% of osseous neoplasms are found in the foot and ankle, 8% of benign soft tissue tumors and 5% of malignant soft tissue tumors are localized to these regions [3]. Similarly, reflected in this issue, the breadth of pathology that affects the foot and ankle is substantial. This, coupled with the anatomic complexity of the foot and ankle, presents challenges to the clinician and imager alike. MR imaging has established itself as an invaluable tool for the non-invasive diagnosis and characterization of foot and ankle evaluation due to its soft-tissue contrast resolution, high spatial resolution and multi-planar capabilities. The purpose of this manuscript will be to offer consideration to state of the art techniques (Table 1) that are currently available on MR vendor platforms, presenting applications that may aid in diagnosis or characterization of disease. In addition, translational techniques (Table 1) will be presented that offer insight into potential future applications that indicate that the true destiny of MR will exceed gross structural evaluation of tissue.

Applications of Currently Available Sequences

Isotropic 3D FSE acquisition for 3D rendering

Historically, most musculoskeletal MR imaging protocols have relied heavily upon 2-dimensional (2D) multi-slice acquisitions, reserving 3-dimensional (3D) volumetric sequences for instances where thinner slice thickness, higher in-plane resolution, reduced volume averaging, and the ability to reconstruct in other planes was desired. The major disadvantages of these sequences were suboptimal soft tissue contrast and long acquisition times [4,5]. More recently, three-dimensional FSE (fast spin echo) sequences have been developed that achieve tissue contrast similar to 2D FSE sequences, in clinically feasible scan times [6,7]. Some version of an isotropic 3D FSE sequence is available on the major MR vendor platforms.

Two major advantages have been leveraged in the literature with regard to implementation of the isotropic 3D FSE sequences. First, the approximation of tissue contrast that approaches 2D FSE techniques provides the possibility for a comprehensive joint assessment with markedly decreased overall scan times (scan once and reformat in any plane) [8,9]. Second, the submillimeter, high-resolution source images allow for detailed evaluation of small, complex anatomic structures [10–13].

Although computed tomography (CT) has traditionally been the imaging method used for the evaluation of bone, both qualitatively and for generating 3D reconstructions, recent developments related to 3D MRI sequences suggest a potential new role for MRI in this regard. Studies are emerging in the literature that establish that MR provides resolution and contrast that allow equal or superior ability as compared to CT to detect osseous pathology such as occult fracture, as well as characterization of fractures required for pre-operative planning [14–17] A few recent studies have addressed the use of 3D MR sequences to generate 3D renderings of bones [18,19]. This is clearly an area of potential development in joints such as the ankle, where complex trauma, articular surface evaluation and bone alignment, among other things, may benefit from 3D visualization of bones (FIG. 1). The capability to provide

this added information from the MR imaging study establishes a sort of ‘one-stop shop’, where the patient can avoid the delay of an added imaging study, the exposure to ionizing radiation, not to mention, better utilization of health care dollars.

MR Neurography

General MR protocols to evaluate peripheral nerves require the ability to detect alteration in nerve signal intensity and morphology, necessitating a combination of sequences that provides high-resolution and sensitivity to mobile water. Acquiring a high quality peripheral nerve MR study that is clinically helpful requires time and attention to detail. Protocols should be planned with all available clinical information as well as electrodiagnostic test results. In many cases, the field of view will have to be tailored to cover a broader area initially for the purposes of screening, followed by smaller field of view 2D and 3D imaging targeted to areas of identified abnormalities. Protocols based upon a combination of T2 and diffusion-weighted imaging (DWI) neurographic sequences have been proposed. These include T1 FSE, T2 adiabatic inversion recovery (IR), proton density (PD), 3-dimensional (3D) IR, and 3D diffusion-weighted reversed fast imaging with steady state precession (DW-PSIF) hybrid pulse sequences [20–22]. The DW-PSIF hybrid pulse sequences provide nerve-selective images, with suppression of adjacent vascular structures, which can be particularly helpful in the foot and ankle (FIG. 2). Diffusion tensor imaging (DTI) is another technique that has been implemented in peripheral nerve evaluation. It exploits the anisotropic properties of axonal fiber tracts, allowing fiber tract mapping as well as calculation of quantitative parameters such as the absolute diffusion coefficient (ADC) [23]. This technique is technically demanding, and has not been broadly adapted for clinical use, but shows great promise for lesion characterization [20,24]. The ADC is a quantitative descriptor of diffusivity and fractional anisotropy (FIG. 3). The mean diffusivity quantifies the average displacement of water molecules, and fractional anisotropy measures the directional preference of the diffusion of the water molecules. If the fractional anisotropy measurement is zero, diffusion is isotropic and can go in any direction (unrestricted), or can go nowhere (completely restricted). If the fractional anisotropy is 1, it means diffusion occurs along only one axis and is fully restricted in all other directions. Neuropathic conditions often result in a decreased fractional anisotropy (increased ADC), where recovering axons often exhibit increased fractional anisotropy (decreased ADC) [23].

Peripheral nerve injury in the foot and ankle is common and can be related to acute trauma, chronic repetitive microtrauma, entrapment syndromes within fibro-osseous tunnels, and post-procedural iatrogenic lesions [25–27]. Nerve sheath tumors and systemic neuropathies can also affect the nerves of the foot and ankle [28–30]. MR criteria (Box 1) for distinguishing a normal versus abnormal nerve include: size (using adjacent vascular structures as an internal standard), signal intensity (isointense to skeletal muscle on T1 and T2, may be minimally hyperintense to muscle with T2 fat suppressed or inversion recovery), preservation of fascicular pattern, smooth course without deviation, preserved perineural fat, normal diffusion tensor tracts, normal fractional anisotropy values (> 0.4 – 0.5), and symmetric brightness on diffusion tensor images [31].

Diffusion-weighted imaging

As indicated in the discussion of peripheral nerve evaluation above, DWI has been studied in the peripheral nervous system, and even more robustly in the central nervous system for some time [32]. Tissue analysis using DWI is based on assumptions that magnitude and direction of local diffusivity in tissue are influenced by the macromolecular environment of diffusing bulk water. Information on tissue structural property is provided by measuring spatial restriction of diffusivity (in contrast to unrestricted diffusion in free water) according to tissue ultrastructure [33]. With conventional DWI, diffusion-sensitizing gradients are applied in a single direction with the subsequent total diffusion movement registration limited to that direction. By combining DWI with diffusion tensor imaging (DTI), several diffusion-sensitizing gradient pairs in different noncoplanar directions are applied, allowing determination of degree of diffusional anisotropy as well as main directions of local diffusion in a tissue [34]. DTI is based on the fact that the magnitude and molecular motion of water will be restricted by structural elements within the tissue, theoretically lending itself to the evaluation of ordered structures such as cartilage and tendon. It has already been implemented in skeletal muscle, bone and musculoskeletal soft tissues [35]. DTI has been proposed as a biomarker for cartilage composition and structure, because of its sensitivity to proteoglycan content through mean diffusivity and to collagen architecture through the fractional anisotropy. It has recently been used to assess postoperative tendon quality in patients with Achilles tendon rupture, providing information regarding the trajectory and tendinous fiber continuity in the repair tissue [36].

The advantages of DTI, as a potential MR biomarker for assessment of articular cartilage, are that it evaluates both proteoglycan and collagen without the need for exogenous contrast material and it does so at a higher resolution than sodium (^{23}Na)-based MR imaging (FIG. 4). In addition, DTI has the ability to assess collagen and proteoglycan independent of each other. The configuration of the collagen fibril network induces anisotropy (measured with fractional anisotropy) of the water molecules. The proteoglycan molecules, however, do not show preferred orientation and therefore restrict motion of water molecules equally in all directions. For this reason, proteoglycan content affects only mean diffusivity. However, diffusion cannot provide a quantitative estimation of the absolute proteoglycan or collagen composition. Further, translation of DWI to the musculoskeletal system has proven difficult for two reasons. First, the relatively short T2 of articular cartilage (20–40 ms) causes low SNR in standard DWI techniques that require long echo times. Second, the sensitivity of DWI to patient motion makes it difficult to achieve the high spatial resolution required for cartilage evaluation [37]. Several recent publications suggest promise for overcoming these technical challenges in patient cohorts [38,39].

Novel MR Pulse Sequences

Ultrashort TE MRI

Ultrashort echo time (UTE) MRI is represented by a group of pulse sequences capable of providing TE values less than 1 millissecond (ms) [40,41]. Conventional MRI sequences employ relatively long echo times, resulting in limited opportunity to encode decaying signal of short T2 tissues before that signal reaches zero. For this reason, biologic tissues whose

intrinsic transverse relaxation times (T2, T2*) are short (generally considered less than 10 ms, though subclassification exists within the 'short' category), appear black, i.e. void of signal on standard MR pulse sequences. By lowering the TE to the range of the intrinsic T2/T2* value of short T2 tissues, signal can be acquired from these tissues, allowing morphologic evaluation. Moreover,, UTE sequences can be used for quantitative evaluation of short T2 tissues. This latter capability will be addressed in the Quantitative MR Imaging section below.

The application of UTE MRI to the musculoskeletal system has been revolutionary, largely due to the short T2 nature of many musculoskeletal tissues. These include the calcified layer of cartilage, fibrocartilaginous structures, ligaments, tendons, and bone [42–46]. The ability to acquire signal and characterize the infrastructure of short T2 tissues presents a paradigm shift in diagnosis and characterization of structural alteration. Rather than being limited to diagnosis of pathology at a point in time when the short T2 tissue has failed through traumatic tearing or severe degeneration, effectively transforming it into a long T2 tissue, UTE MRI affords the opportunity to identify pathologic changes at an earlier stage, which provides the chance for earlier intervention and controlled treatment. The UTE MRI sequences currently have limited availability on vendor platforms, but promising results have been introduced in the literature for clinical application of these sequences in setting of meniscal repair, cartilage repair and osteoarthrosis [47–49].

Potential applications for UTE MRI could include evaluation of osteochondral injury, assessment of degenerative changes, and monitoring of tissue healing. Ankle sprains have an estimated daily occurrence of 27,000 in the United States, with 50% leading to osteochondral lesions [50]. UTE MRI allows assessment of the calcified layer of cartilage at the talar dome, helping to characterize osteochondral junction injury acutely and in follow up (FIG. 5). Further, bone marrow-stimulating techniques (abrasion, drilling, microfracture) are used to treat chondral defects [51]. In such procedures, it is important to assess the presence and nature of fill tissue at the repair site, as well to assess the reconstitution of the cartilage-bone interface [52].

In addition, UTE MRI is well suited to evaluate ankle tendons, both tensile components and entheseal attachments to bone (FIGS. 5, 6). Achilles tendinopathy is the most common cause of posterior heel pain, and is often due to mechanical stress related to overload or overuse of the muscle-tendon unit [53]. Recently, overuse conditions in the Achilles tendon have been associated with non-uniform mechanical loading of the triceps surae (lateral gastrocnemius, medial gastrocnemius, soleus) [54]. UTE MRI offers the ability to identify the distribution of the relative contributions of the Achilles tendon, as well as the ability to identify structural alteration through loss of the normal fascicular appearance of the tendon (FIG. 7)

The entheseal attachment of the Achilles tendon also has great interest from a clinical standpoint. It is suggested in the literature that there is a significant cohort of seronegative spondyloarthropathy patients that have subclinical disease involving the lower limb [55,56]. UTE MRI is well suited to characterize the normal appearance of the Achilles tendon synovioentheseal complex, as well as alterations that may reflect early changes of subclinical entheseal disease [57] (FIG. 5).

Quantitative MR Imaging Biomarkers

MR based techniques have been developed that allow characterization and quantification of the biochemical composition of tissue. This has been a revolutionary step forward in musculoskeletal MR, allowing non-invasive assessment of biochemical and structural tissue status at very early stages of disease as well as in repair tissue. The quantitative nature offers an objective data point that will undoubtedly prove important in guiding treatment, developing new treatment options, and perhaps serving as surrogate for tissue material property.

The majority of quantitative biomarkers in the musculoskeletal system have been aimed at collagen and proteoglycan evaluation, as they are major structural elements in most musculoskeletal tissues. Further, much of the initial biomarker work was performed in articular cartilage, and has expanded rapidly to application in other musculoskeletal tissues. For the purposes of potential applications of quantitative biomarkers in the foot and ankle, the following discussion will focus on evaluation of tendon and cartilage. In tendons, quantitative assessment has focused on collagen content, rather than proteoglycan evaluation because proteoglycans represent a small percentage of the overall dry weight of tendons (0.2 – 5%), as compared to articular cartilage (12%) [58,59].

Collagen Evaluation

T2 mapping—T2 relaxation times represent the rate of constant proton dephasing after an initial radiofrequency pulse is delivered. The T2 relaxation value of articular cartilage reflects water content, collagen content and collagen fiber orientation in the extracellular matrix, with longer T2 relaxation values representing cartilage degeneration [60,61]. T2 relaxation data is acquired using a constant TR-variable TE technique, in which signal intensities from regions of interest are plotted against TE, resulting in a map of T2 relaxation times within the tissue. A zonal variation in T2 values has been shown in articular cartilage due to the densely packed nature of the collagen fibers in the deeper layers of articular cartilage. This limits mobility of protons, and results in a lower T2 value in the deeper cartilage layers [62]. Further, at the junction of cartilage and bone, the calcified layer of cartilage has a very short T2 relaxation time, making T2 measurements unreliable in this region [42,63].

A T2 mapping pulse sequence is available on most vendor platforms. Extensive studies have shown this form of T2 quantification to be reproducible and have shown the validity of the measurements [60,64,65]. The technique has been used in many clinical studies that have explored articular cartilage in the context of osteoarthrosis, malalignment, and trauma [60,66]. T2 mapping has been also been widely used in the evaluation of ankle articular cartilage (FIG. 8). Studies performed in the ankle, similar to those performed in the knee, have focused on structure, post-traumatic changes, evaluation of repair tissue, and exploration of novel techniques such as traction in the foot and ankle to improve visualization and thereby improve quantification [67–71].

UTE T2* mapping—T2* relaxation time is dependent on interactions between spins, tissue hydration and susceptibility [41]. Similar to T2 mapping, quantification is performed

with a constant TR and variable TE technique. However, T2* mapping utilizes UTE sequences, allowing much shorter TE ranges to be exploited (lowest TE in the microsecond to 1 ms range). Studies applying UTE T2* mapping suggest that the evaluation of short T2 tissues by methods that operate in a short T2 range offer more sensitive evaluation of structural alteration. UTE T2* mapping is most effectively applied to short T2 tissues (FIG. 8). To date, clinical feasibility has been shown in the evaluation of articular cartilage in the knee and hip [47,72–77].

Quantitative T2* mapping of tendon, specifically the Achilles tendon, has been performed in animal models and in ex vivo and in vivo human tissue [78–83]. Much of this work has been performed with T2* or UTE T2* techniques that allow identification of long and short T2 tissue fractions. The tendon appears to have a complex composition, with significant long and short T2 components, necessitating care in interpretation of the quantitative data (FIG. 6). Exciting work suggests that quantitative measures may have the potential to serve as a reference standard for mechanical property of tissue [84]. From a practical standpoint, the prediction of tissue material property and function over time may prove far more important than the detection of structural alteration (FIG. 9).

Proteoglycan Evaluation

T1 rho MRI—T1 rho (the spin-lattice relaxation time in the rotating frame), is a technique that has been used to assess low-frequency interactions between hydrogen and macromolecules in free water. It uses clusters of radiofrequency pulses to lock magnetization in the transverse plane, followed by additional radiofrequency pulses to drive longitudinal recovery [85]. T1 rho probes slow motion interactions between motion-restricted water molecules and their local macromolecular environment. In vitro studies demonstrated that depletion of proteoglycan resulted in increased T1 rho values, suggesting T1 rho estimates proteoglycan content [86,87]. There is some evidence that other factors, including collagen fiber orientation and concentration of other macromolecules, may contribute to T1 rho values [88]. It appears, however, that T1 rho may be more sensitive than T2 mapping for differentiating between normal cartilage and early-stage OA [89]. This raises the possibility that proteoglycan loss may precede collagen degradation in OA, and further suggests T1 rho may provide a better measure.

T1 rho has been employed extensively in patient cohorts, primarily focusing on the knee. Studies have emphasized T1 rho as a biomarker in articular cartilage representing early degenerative changes in the joint, a potential surrogate for altered meniscal function, and altered mechanical axis of load distribution in weight bearing in the ACL-reconstructed knee [90–93]. While this technique has not been described in the ankle articular cartilage, clearly it holds similar potential to the knee (FIG. 10).

Sodium MRI and ultra high field MRI (7T)—MRI at ultra-high field (7 T) offers high signal-to-noise ratio, which can be used beneficially in several different musculoskeletal applications. Spatial resolution in morphological imaging of small structures, such as those found in the foot and ankle, can be significantly improved. In addition, imaging techniques that suffer from low signal-to-noise ratio and low sensitivity can offset these relative

disadvantages through partnering with ultra high field MR. Sodium (^{23}Na) MRI is one such technique (FIG. 11). As its name implies, ^{23}Na MRI is based upon the detection of sodium ions in tissues (requiring an RF coil tuned to sodium), allowing quantification of their concentration. In musculoskeletal tissues, sodium ions balance the fixed negative charge of the glycosaminoglycan side chains of proteoglycan molecules, making sodium ion concentration a biomarker for proteoglycan concentration. One major strength of this technique is its strong correlation with glycosaminoglycan concentration in cartilage [94].

In vivo application of ^{23}Na-imaging has been performed in articular cartilage, skeletal muscle, and tendon [95–98].

Functional Assessment of Tissue

Kinematic MRI

MR application in the musculoskeletal system has evolved significantly to emerge as a non-invasive imaging study that can provide a global structural evaluation. As noted, pulse sequence development provides not only excellent soft tissue analysis, but rivals CT for the evaluation of bone. Quantitative imaging techniques may offer insight into tissue biochemistry and even material property. An additional frontier to address with regard to musculoskeletal MR is the dynamic nature of the system. Patients are imaged in static positions, though injury is incurred dynamically. Further, joint instability will not likely be apparent in static images.

Methodology has developed and been applied to the musculoskeletal system to allow for real time evaluation through range-of-motion using ultrafast MRI scans (FIG. 12). The degree of motion is limited by the physical constraints of the scanner, but studies have been described in various joints, including the ankle [99–103]. The ability to dynamically evaluate a joint, while visualizing static and dynamic stabilizers, would be a valuable tool in providing targeted and effective diagnosis and ultimate treatment.

References

1. Sharma GK, Dhillon MS, Dhatt SS. The influence of foot and ankle injury patterns and treatment delays on outcomes in a tertiary hospital; a one-year prospective observation. Foot (Edinb). 2016; 26:48. [PubMed: 26895255]
2. Hicks CW, Selvarajah S, Mathioudakis N, et al. Burden of Infected Diabetic Foot Ulcers on Hospital Admissions and Costs. Ann Vasc Surg. 2016
3. Kennedy JG, Ross KA, Smyth NA, et al. Primary Tumors of the Foot and Ankle. Foot Ankle Spec. 2016; 9:58. [PubMed: 26644034]
4. Gold GE, Busse RF, Beehler C, et al. Isotropic MRI of the knee with 3D fast spin-echo extended echo-train acquisition (XETA): initial experience. AJR Am J Roentgenol. 2007; 188:1287. [PubMed: 17449772]
5. Notohamiprodjo M, Horng A, Pietschmann MF, et al. MRI of the knee at 3T: first clinical results with an isotropic PDfs-weighted 3D–TSE-sequence. Invest Radiol. 2009; 44:585. [PubMed: 19668001]
6. Busse RF, Brau AC, Vu A, et al. Effects of refocusing flip angle modulation and view ordering in 3D fast spin echo. Magn Reson Med. 2008; 60:640. [PubMed: 18727082]

7. Busse RF, Hariharan H, Vu A, et al. Fast spin echo sequences with very long echo trains: design of variable refocusing flip angle schedules and generation of clinical T2 contrast. Magn Reson Med. 2006; 55:1030. [PubMed: 16598719]
8. Kijowski R, Davis KW, Woods MA, et al. Knee joint: comprehensive assessment with 3D isotropic resolution fast spin-echo MR imaging--diagnostic performance compared with that of conventional MR imaging at 3.0 T. Radiology. 2009; 252:486. [PubMed: 19703886]
9. Rosas H, Kijowski R. Volumetric magnetic resonance imaging of the musculoskeletal system. Semin Roentgenol. 2013; 48:140. [PubMed: 23452461]
10. Notohamiprodjo M, Kuschel B, Horng A, et al. 3D–MRI of the ankle with optimized 3D–SPACE. Invest Radiol. 2012; 47:231. [PubMed: 22373531]
11. Park HJ, Lee SY, Park NH, et al. Three-dimensional isotropic T2-weighted fast spin-echo (VISTA) ankle MRI versus two-dimensional fast spin-echo T2-weighted sequences for the evaluation of anterior talofibular ligament injury. Clin Radiol. 2016; 71:349. [PubMed: 26774370]
12. Sutherland JK, Nozaki T, Kaneko Y, et al. Initial experience with 3D isotropic high-resolution 3 T MR arthrography of the wrist. BMC Musculoskelet Disord. 2016; 17:30. [PubMed: 26772813]
13. Yi J, Cha JG, Lee YK, et al. MRI of the anterior talofibular ligament, talar cartilage and os subfibulare: Comparison of isotropic resolution 3D and conventional 2D T2-weighted fast spin-echo sequences at 3.0 T. Skeletal Radiol. 2016
14. Yin ZG, Zhang JB, Kan SL, et al. Diagnostic accuracy of imaging modalities for suspected scaphoid fractures: meta-analysis combined with latent class analysis. J Bone Joint Surg Br. 2012; 94:1077. [PubMed: 22844049]
15. Hakkarinen DK, Banh KV, Hendey GW. Magnetic resonance imaging identifies occult hip fractures missed by 64-slice computed tomography. J Emerg Med. 2012; 43:303. [PubMed: 22459594]
16. Collin D, Geijer M, Gothlin JH. Computed tomography compared to magnetic resonance imaging in occult or suspect hip fractures. A retrospective study in 44 patients. Eur Radiol. 20162016
17. Gyftopoulos S, Hasan S, Bencardino J, et al. Diagnostic accuracy of MRI in the measurement of glenoid bone loss. AJR Am J Roentgenol. 2012; 199:873. [PubMed: 22997381]
18. Gyftopoulos S, Yemin A, Mulholland T, et al. 3DMR osseous reconstructions of the shoulder using a gradient-echo based two-point Dixon reconstruction: a feasibility study. Skeletal Radiol. 2013; 42:347. [PubMed: 22829026]
19. Glaser C, D'Anastasi M, Theisen D, et al. Understanding 3D TSE Sequences: Advantages, Disadvantages, and Application in MSK Imaging. Semin Musculoskelet Radiol. 2015; 19:321. [PubMed: 26583360]
20. Chhabra A, Andreisek G, Soldatos T, et al. MR neurography: past, present, and future. AJR Am J Roentgenol. 2011; 197:583. [PubMed: 21862800]
21. Chhabra A, Lee PP, Bizzell C, et al. 3 Tesla MR neurography--technique, interpretation, and pitfalls. Skeletal Radiol. 2011; 40:1249. [PubMed: 21547613]
22. Chhabra A, Soldatos T, Subhawong TK, et al. The application of three-dimensional diffusion-weighted PSIF technique in peripheral nerve imaging of the distal extremities. J Magn Reson Imaging. 2011; 34:962. [PubMed: 21769979]
23. Burge AJ, Gold SL, Kuong S, et al. High-resolution magnetic resonance imaging of the lower extremity nerves. Neuroimaging Clin N Am. 2014; 24:151. [PubMed: 24210318]
24. Simon NG, Lagopoulos J, Gallagher T, et al. Peripheral nerve diffusion tensor imaging is reliable and reproducible. J Magn Reson Imaging. 2016; 43:962. [PubMed: 26397723]
25. Thordarson DB, Shean CJ. Nerve and tendon lacerations about the foot and ankle. J Am Acad Orthop Surg. 2005; 13:186. [PubMed: 15938607]
26. Lopez-Ben R. Imaging of nerve entrapment in the foot and ankle. Foot Ankle Clin. 2011; 16:213. [PubMed: 21600443]
27. Chhabra A, Williams EH, Wang KC, et al. MR neurography of neuromas related to nerve injury and entrapment with surgical correlation. AJNR Am J Neuroradiol. 2010; 31:1363. [PubMed: 20133388]
28. Carvajal JA, Cuartas E, Qadir R, et al. Peripheral nerve sheath tumors of the foot and ankle. Foot Ankle Int. 2011; 32:163. [PubMed: 21288416]

29. Pham M, Oikonomou D, Hornung B, et al. Magnetic resonance neurography detects diabetic neuropathy early and with Proximal Predominance. Ann Neurol. 2015; 78:939. [PubMed: 26381658]
30. Kollmer J, Hund E, Hornung B, et al. In vivo detection of nerve injury in familial amyloid polyneuropathy by magnetic resonance neurography. Brain. 2015; 138:549. [PubMed: 25526974]
31. Chhabra A. Peripheral MR neurography: approach to interpretation. Neuroimaging Clin N Am. 2014; 24:79. [PubMed: 24210314]
32. Pierpaoli C, Jezzard P, Basser PJ, et al. Diffusion tensor MR imaging of the human brain. Radiology. 1996; 201:637. [PubMed: 8939209]
33. Glaser C. New techniques for cartilage imaging: T2 relaxation time and diffusion-weighted MR imaging. Radiol Clin North Am. 2005; 43:641. [PubMed: 15893528]
34. Le Bihan D, Mangin JF, Poupon C, et al. Diffusion tensor imaging: concepts and applications. J Magn Reson Imaging. 2001; 13:534. [PubMed: 11276097]
35. Bhojwani N, Szpakowski P, Partovi S, et al. Diffusion-weighted imaging in musculoskeletal radiology-clinical applications and future directions. Quant Imaging Med Surg. 2015; 5:740. [PubMed: 26682143]
36. Sarman H, Atmaca H, Cakir O, et al. Assessment of Postoperative Tendon Quality in Patients With Achilles Tendon Rupture Using Diffusion Tensor Imaging and Tendon Fiber Tracking. J Foot Ankle Surg. 2015; 54:782. [PubMed: 25736446]
37. Miller KL, Hargreaves BA, Gold GE, et al. Steady-state diffusion-weighted imaging of in vivo knee cartilage. Magn Reson Med. 2004; 51:394. [PubMed: 14755666]
38. Apprich S, Trattnig S, Welsch GH, et al. Assessment of articular cartilage repair tissue after matrix-associated autologous chondrocyte transplantation or the microfracture technique in the ankle joint using diffusion-weighted imaging at 3 Tesla. Osteoarthritis Cartilage. 2012; 20:703. [PubMed: 22445916]
39. Raya JG, Dettmann E, Notohamiprodjo M, et al. Feasibility of in vivo diffusion tensor imaging of articular cartilage with coverage of all cartilage regions. Eur Radiol. 2014; 24:1700. [PubMed: 24816930]
40. Bydder GM. Review. The Agfa Mayneord lecture: MRI of short and ultrashort T(2) and T(2)* components of tissues, fluids and materials using clinical systems. Br J Radiol. 2011; 84:1067. [PubMed: 22101579]
41. Chang EY, Du J, Chung CB. UTE imaging in the musculoskeletal system. J Magn Reson Imaging. 2015; 41:870. [PubMed: 25045018]
42. Bae WC, Dwek JR, Znamirowski R, et al. Ultrashort echo time MR imaging of osteochondral junction of the knee at 3 T: identification of anatomic structures contributing to signal intensity. Radiology. 2010; 254:837. [PubMed: 20177096]
43. Gatehouse PD, He T, Puri BK, et al. Contrast-enhanced MRI of the menisci of the knee using ultrashort echo time (UTE) pulse sequences: imaging of the red and white zones. Br J Radiol. 2004; 77:641. [PubMed: 15326040]
44. Sanal HT, Bae WC, Pauli C, et al. Magnetic resonance imaging of the temporomandibular joint disc: feasibility of novel quantitative magnetic resonance evaluation using histologic and biomechanical reference standards. J Orofac Pain. 2011; 25:345. [PubMed: 22247930]
45. Han M, Larson PE, Liu J, et al. Depiction of achilles tendon microstructure in vivo using high-resolution 3-dimensional ultrashort echo-time magnetic resonance imaging at 7 T. Invest Radiol. 2014; 49:339. [PubMed: 24500089]
46. Bae WC, Chen PC, Chung CB, et al. Quantitative ultrashort echo time (UTE) MRI of human cortical bone: correlation with porosity and biomechanical properties. J Bone Miner Res. 2012; 27:848. [PubMed: 22190232]
47. Sneag DB, Shah P, Koff MF, et al. Quantitative Ultrashort Echo Time Magnetic Resonance Imaging Evaluation of Postoperative Menisci: a Pilot Study. HSS J. 2015; 11:123. [PubMed: 26140031]
48. Chu CR, Williams AA, West RV, et al. Quantitative Magnetic Resonance Imaging UTE-T2* Mapping of Cartilage and Meniscus Healing After Anatomic Anterior Cruciate Ligament Reconstruction. Am J Sports Med. 2014; 42:1847. [PubMed: 24812196]

49. McWalter EJ, Gold GE. UTE T2 * mapping detects sub-clinical meniscus degeneration. Osteoarthritis Cartilage. 2012; 20:471. [PubMed: 22406647]
50. Savage-Elliott I, Ross KA, Smyth NA, et al. Osteochondral lesions of the talus: a current concepts review and evidence-based treatment paradigm. Foot Ankle Spec. 2014; 7:414. [PubMed: 25100765]
51. Domayer SE, Welsch GH, Stelzeneder D, et al. Microfracture in the Ankle: Clinical Results and MRI with T2-Mapping at 3.0 T after 1 to 8 Years. Cartilage. 2011; 2:73. [PubMed: 26069571]
52. Chen H, Chevrier A, Hoemann CD, et al. Characterization of subchondral bone repair for marrow-stimulated chondral defects and its relationship to articular cartilage resurfacing. Am J Sports Med. 2011; 39:1731. [PubMed: 21628638]
53. Berner J, Zufferey P. [Achilles tendinopathy]. Rev Med Suisse. 2015; 11:606. [PubMed: 25946872]
54. Toumi H, Larguech G, Cherief M, et al. Implications of the calf musculature and Achilles tendon architectures for understanding the site of injury. J Biomech. 2016
55. Bandinelli F, Prignano F, Bonciani D, et al. Ultrasound detects occult entheseal involvement in early psoriatic arthritis independently of clinical features and psoriasis severity. Clin Exp Rheumatol. 2013; 31:219. [PubMed: 23190740]
56. Gisondi P, Tinazzi I, El-Dalati G, et al. Lower limb enthesopathy in patients with psoriasis without clinical signs of arthropathy: a hospital-based case-control study. Ann Rheum Dis. 2008; 67:26. [PubMed: 17720726]
57. Du J, Chiang AJ, Chung CB, et al. Orientational analysis of the Achilles tendon and enthesis using an ultrashort echo time spectroscopic imaging sequence. Magn Reson Imaging. 2010; 28:178. [PubMed: 19695811]
58. Sophia Fox AJ, Bedi A, Rodeo SA. The basic science of articular cartilage: structure, composition, and function. Sports Health. 2009; 1:461. [PubMed: 23015907]
59. Amiel D, Frank C, Harwood F, et al. Tendons and ligaments: a morphological and biochemical comparison. J Orthop Res. 1984; 1:257. [PubMed: 6481509]
60. Nissi MJ, Rieppo J, Toyras J, et al. T(2) relaxation time mapping reveals age-and species-related diversity of collagen network architecture in articular cartilage. Osteoarthritis Cartilage. 2006; 14:1265. [PubMed: 16843689]
61. Mosher TJ, Smith H, Dardzinski BJ, et al. MR imaging and T2 mapping of femoral cartilage: in vivo determination of the magic angle effect. AJR Am J Roentgenol. 2001; 177:665. [PubMed: 11517068]
62. Carballido-Gamio J, Blumenkrantz G, Lynch JA, et al. Longitudinal analysis of MRI T(2) knee cartilage laminar organization in a subset of patients from the osteoarthritis initiative. Magn Reson Med. 2010; 63:465. [PubMed: 19918905]
63. Bae WC, Biswas R, Chen K, et al. UTE MRI of the Osteochondral Junction. Curr Radiol Rep. 2014; 2:35. [PubMed: 25061547]
64. Dunn TC, Lu Y, Jin H, et al. T2 relaxation time of cartilage at MR imaging: comparison with severity of knee osteoarthritis. Radiology. 2004; 232:592. [PubMed: 15215540]
65. Mosher TJ, Zhang Z, Reddy R, et al. Knee articular cartilage damage in osteoarthritis: analysis of MR image biomarker reproducibility in ACRIN-PA 4001 multicenter trial. Radiology. 2011; 258:832. [PubMed: 21212364]
66. Friedrich KM, Shepard T, Chang G, et al. Does joint alignment affect the T2 values of cartilage in patients with knee osteoarthritis? Eur Radiol. 2010; 20:1532. [PubMed: 20013272]
67. Juras V, Zbyn S, Mlynarik V, et al. The compositional difference between ankle and knee cartilage demonstrated by T2 mapping at 7 Tesla MR. Eur J Radiol. 2016; 85:771. [PubMed: 26971422]
68. Lim Y, Cha JG, Yi J, et al. Topographical and sex variations in the T2 relaxation times of articular cartilage in the ankle joints of healthy young adults using 3.0T MRI. J Magn Reson Imaging. 2016; 43:455. [PubMed: 26219078]
69. Golditz T, Steib S, Pfeifer K, et al. Functional ankle instability as a risk factor for osteoarthritis: using T2-mapping to analyze early cartilage degeneration in the ankle joint of young athletes. Osteoarthritis Cartilage. 2014; 22:1377. [PubMed: 24814687]

70. Kubosch EJ, Erdle B, Izadpanah K, et al. Clinical outcome and T2 assessment following autologous matrix-induced chondrogenesis in osteochondral lesions of the talus. Int Orthop. 2016; 40:65. [PubMed: 26346373]
71. Jungmann PM, Baum T, Schaeffeler C, et al. 3.0T MR imaging of the ankle: Axial traction for morphological cartilage evaluation, quantitative T2 mapping and cartilage diffusion imaging-A preliminary study. Eur J Radiol. 2015; 84:1546. [PubMed: 26003193]
72. Williams A, Qian Y, Bear D, et al. Assessing degeneration of human articular cartilage with ultra-short echo time (UTE) T2* mapping. Osteoarthritis Cartilage. 2010; 18:539. [PubMed: 20170769]
73. Williams A, Qian Y, Chu CR. UTE-T2 * mapping of human articular cartilage in vivo: a repeatability assessment. Osteoarthritis Cartilage. 2011; 19:84. [PubMed: 21035556]
74. Williams A, Qian Y, Golla S, et al. UTE-T2 * mapping detects sub-clinical meniscus injury after anterior cruciate ligament tear. Osteoarthritis Cartilage. 2012; 20:486. [PubMed: 22306000]
75. Bittersohl B, Hosalkar HS, Hughes T, et al. Feasibility of T2* mapping for the evaluation of hip joint cartilage at 1.5T using a three-dimensional (3D), gradient-echo (GRE) sequence: a prospective study. Magn Reson Med. 2009; 62:896. [PubMed: 19645008]
76. Bittersohl B, Miese FR, Hosalkar HS, et al. T2* mapping of hip joint cartilage in various histological grades of degeneration. Osteoarthritis Cartilage. 2012; 20:653. [PubMed: 22469845]
77. Miese FR, Zilkens C, Holstein A, et al. Assessment of early cartilage degeneration after slipped capital femoral epiphysis using T2 and T2* mapping. Acta Radiol. 2011; 52:106. [PubMed: 20954816]
78. Fukawa T, Yamaguchi S, Watanabe A, et al. Quantitative Assessment of Tendon Healing by Using MR T2 Mapping in a Rabbit Achilles Tendon Transection Model Treated with Platelet-rich Plasma. Radiology. 2015; 276:748. [PubMed: 25816105]
79. Wang N, Xia Y. Anisotropic analysis of multi-component T2 and T1rho relaxations in achilles tendon by NMR spectroscopy and microscopic MRI. J Magn Reson Imaging. 2013; 38:625. [PubMed: 23349070]
80. Filho GH, Du J, Pak BC, et al. Quantitative characterization of the Achilles tendon in cadaveric specimens: T1 and T2* measurements using ultrashort-TE MRI at 3 T. AJR Am J Roentgenol. 2009; 192:W117. [PubMed: 19234239]
81. Juras V, Apprich S, Pressl C, et al. Histological correlation of 7 T multi-parametric MRI performed in ex-vivo Achilles tendon. Eur J Radiol. 2013; 82:740. [PubMed: 22177325]
82. Chang EY, Du J, Statum S, et al. Quantitative bi-component T2* analysis of histologically normal Achilles tendons. Muscles Ligaments Tendons J. 2015; 5:58. [PubMed: 26261782]
83. Juras V, Apprich S, Szomolanyi P, et al. Bi-exponential T2 analysis of healthy and diseased Achilles tendons: an in vivo preliminary magnetic resonance study and correlation with clinical score. Eur Radiol. 2013; 23:2814. [PubMed: 23760303]
84. Koff MF, Pownder SL, Shah PH, et al. Ultrashort echo imaging of cyclically loaded rabbit patellar tendon. J Biomech. 2014; 47:3428. [PubMed: 25234349]
85. Potter HG, Black BR, Chong le R. New techniques in articular cartilage imaging. Clin Sports Med. 2009; 28:77. [PubMed: 19064167]
86. Akella SV, Regatte RR, Gougoutas AJ, et al. Proteoglycan-induced changes in T1rho-relaxation of articular cartilage at 4T. Magn Reson Med. 2001; 46:419. [PubMed: 11550230]
87. Guermazi A, Alizai H, Crema MD, et al. Compositional MRI techniques for evaluation of cartilage degeneration in osteoarthritis. Osteoarthritis Cartilage. 2015; 23:1639. [PubMed: 26050864]
88. Mlynarik V, Trattnig S, Huber M, et al. The role of relaxation times in monitoring proteoglycan depletion in articular cartilage. J Magn Reson Imaging. 1999; 10:497. [PubMed: 10508315]
89. Stahl R, Luke A, Li X, et al. T1rho, T2 and focal knee cartilage abnormalities in physically active and sedentary healthy subjects versus early OA patients--a 3.0-Tesla MRI study. Eur Radiol. 2009; 19:132. [PubMed: 18709373]
90. Bolbos RI, Zuo J, Banerjee S, et al. Relationship between trabecular bone structure and articular cartilage morphology and relaxation times in early OA of the knee joint using parallel MRI at 3 T. Osteoarthritis Cartilage. 2008; 16:1150. [PubMed: 18387828]

91. Zarins ZA, Bolbos RI, Pialat JB, et al. Cartilage and meniscus assessment using T1rho and T2 measurements in healthy subjects and patients with osteoarthritis. Osteoarthritis Cartilage. 2010; 18:1408. [PubMed: 20696262]
92. Nishioka H, Hirose J, Nakamura E, et al. Detecting ICRS grade 1 cartilage lesions in anterior cruciate ligament injury using T1rho and T2 mapping. Eur J Radiol. 2013; 82:1499. [PubMed: 23743050]
93. Souza RB, Feeley BT, Zarins ZA, et al. T1rho MRI relaxation in knee OA subjects with varying sizes of cartilage lesions. Knee. 2013; 20:113. [PubMed: 23159719]
94. Madelin G, Poidevin F, Makrymallis A, et al. Classification of sodium MRI data of cartilage using machine learning. Magn Reson Med. 2015; 74:1435. [PubMed: 25367844]
95. Zbyn S, Mlynarik V, Juras V, et al. Evaluation of cartilage repair and osteoarthritis with sodium MRI. NMR Biomed. 2016; 29:206. [PubMed: 25810325]
96. Newbould RD, Miller SR, Tielbeek JA, et al. Reproducibility of sodium MRI measures of articular cartilage of the knee in osteoarthritis. Osteoarthritis Cartilage. 2012; 20:29. [PubMed: 22040861]
97. Madelin G, Regatte RR. Biomedical applications of sodium MRI in vivo. J Magn Reson Imaging. 2013; 38:511. [PubMed: 23722972]
98. Juras V, Zbyn S, Pressl C, et al. Sodium MR imaging of Achilles tendinopathy at 7 T: preliminary results. Radiology. 2012; 262:199. [PubMed: 22056685]
99. Borotikar BS, Sheehan FT. In vivo patellofemoral contact mechanics during active extension using a novel dynamic MRI-based methodology. Osteoarthritis Cartilage. 2013; 21:1886. [PubMed: 24012620]
100. Borotikar BS, Sipprell WH 3rd, Wible EE, et al. A methodology to accurately quantify patellofemoral cartilage contact kinematics by combining 3D image shape registration and cine-PC MRI velocity data. J Biomech. 2012; 45:1117. [PubMed: 22284428]
101. Draper CE, Besier TF, Santos JM, et al. Using real-time MRI to quantify altered joint kinematics in subjects with patellofemoral pain and to evaluate the effects of a patellar brace or sleeve on joint motion. J Orthop Res. 2009; 27:571. [PubMed: 18985690]
102. Fei Z, Fan C, Ngo S, et al. Dynamic evaluation of cervical disc herniation using kinetic MRI. J Clin Neurosci. 2011; 18:232. [PubMed: 21159511]
103. Clarke EC, Martin JH, d'Entremont AG, et al. A non-invasive, 3D, dynamic MRI method for measuring muscle moment arms in vivo: demonstration in the human ankle joint and Achilles tendon. Med Eng Phys. 2015; 37:93. [PubMed: 25466777]

Box 1

Criteria for normal nerve on diffusion tensor MR images

MR Criteria for a Normal Nerve
Size, using adjacent vascular structures as an internal standard
Signal Intensity isointense to skeletal muscle on T1 and T2 (may be minimally hyperintense to muscle with T2 fat suppressed or inversion recovery)
Preservation of fascicular pattern
Smooth course without deviation
Preservation of perineural fat
Normal diffusion tensor tracts
Normal fractional anisotropy values >0.4 to 0.5
Symmetric brightness on diffusion tensor images

Key Points

1. Isotropic 3D MR imaging provides comprehensive joint assessment by offering exquisite submillimeter anatomic detail while maintaining soft tissue contrast comparable to conventional 2D sequences.
2. MR neurography leverages FSE and DWI techniques to provide high resolution, nerve-selective images for assessing peripheral nerve injuries of the foot and ankle.
3. Advanced tools for characterizing the structural integrity of cartilage, tendon and bone include ultrashort TE MRI, quantitative MRI, and diffusion tensor imaging.
4. Sodium imaging with ultra-high field strength MRI holds future promise for assessing structural properties such as the glycosaminoglycan content of articular cartilage.

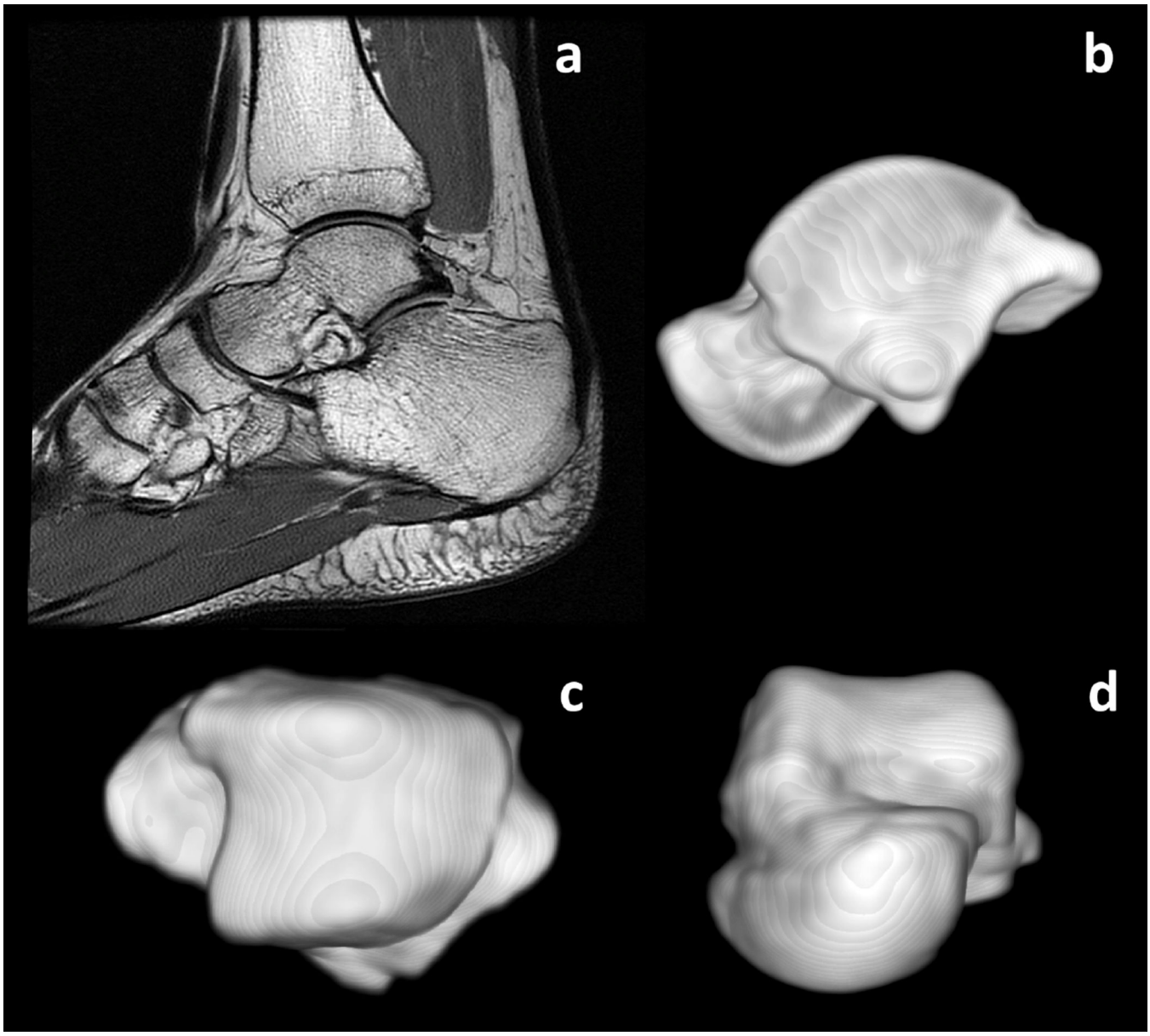

Figure 1.

(**a**) High resolution 3D FSE image of an ankle in sagittal plane, taken at FOV=140 mm, matrix=320×320, slice=0.5 mm, TR=800 ms, TE=19, ETL=28. The talus (arrow) was segmented to render a 3D model shown in (**b**) sagittal, (**c**) axial, and (**d**) coronal views.

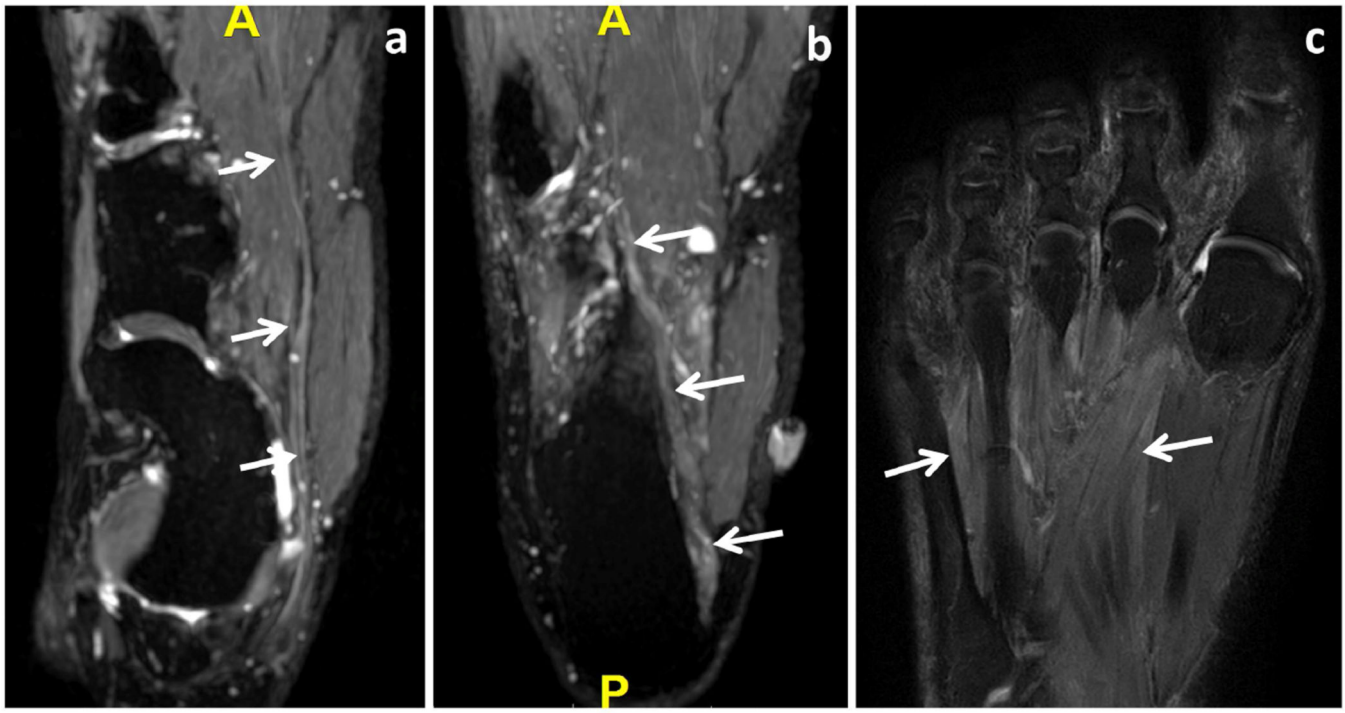

Figure 2.

Ankle MR neurography. Adult male with medial ankle pain following plantar fascial release. (**a**) Coronal 3D DW PSIF MIP image shows normal intermediate signal appearance of the medial plantar nerve (arrows). (**b**) More plantar image shows irregular contoured and thickened lateral plantar nerve (arrows) with distal hyperintensity in keeping with Sunderland class III injury. (**c**) Horizontal long axis T2 SPAIR image shows lateral compartment edema like signal in keeping with muscle denervation changes (arrows). *Images courtesy of Dr. Vibhor Wadhwa, Radiology intern and Dr. Avneesh Chhabra, Associate Professor Radiology & Orthopedic Surgery, University of Texas Southwestern Medical Center, Dallas, TX.*

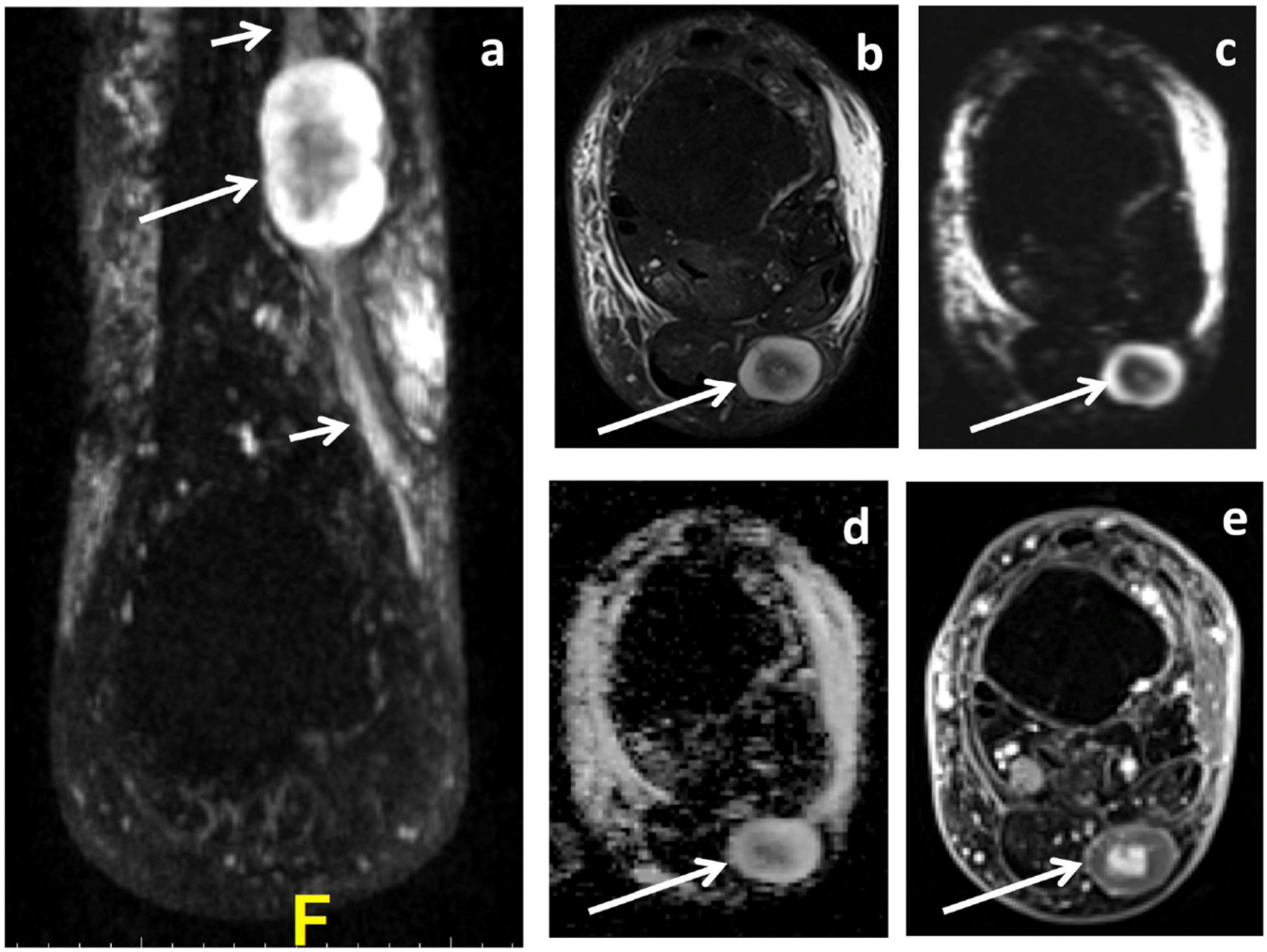

Figure 3.

MR neurography with DTI. (**a**) Coronal 3D DW PSIF MIP image shows sural nerve (small arrows) with associated peripheral nerve sheath tumor (pathology proven neurofibroma, large arrow). (**b**) Axial T2 SPAIR, (**c**) Trace image (reflects global diffusion magnitude calculated from diffusion images obtained with diffusion gradients in at least 3 different spatial directions), (**d**) ADC image, and (**e**) post contrast image. Notice target appearance on all images (long arrows) with high ADC=2.0×10^{-3} mm^2/s consistent with a benign lesion. *Images courtesy of Dr. Vibhor Wadhwa, Radiology intern and Dr. Avneesh Chhabra, Associate Professor Radiology & Orthopedic Surgery, University of Texas Southwestern Medical Center, Dallas, TX.*

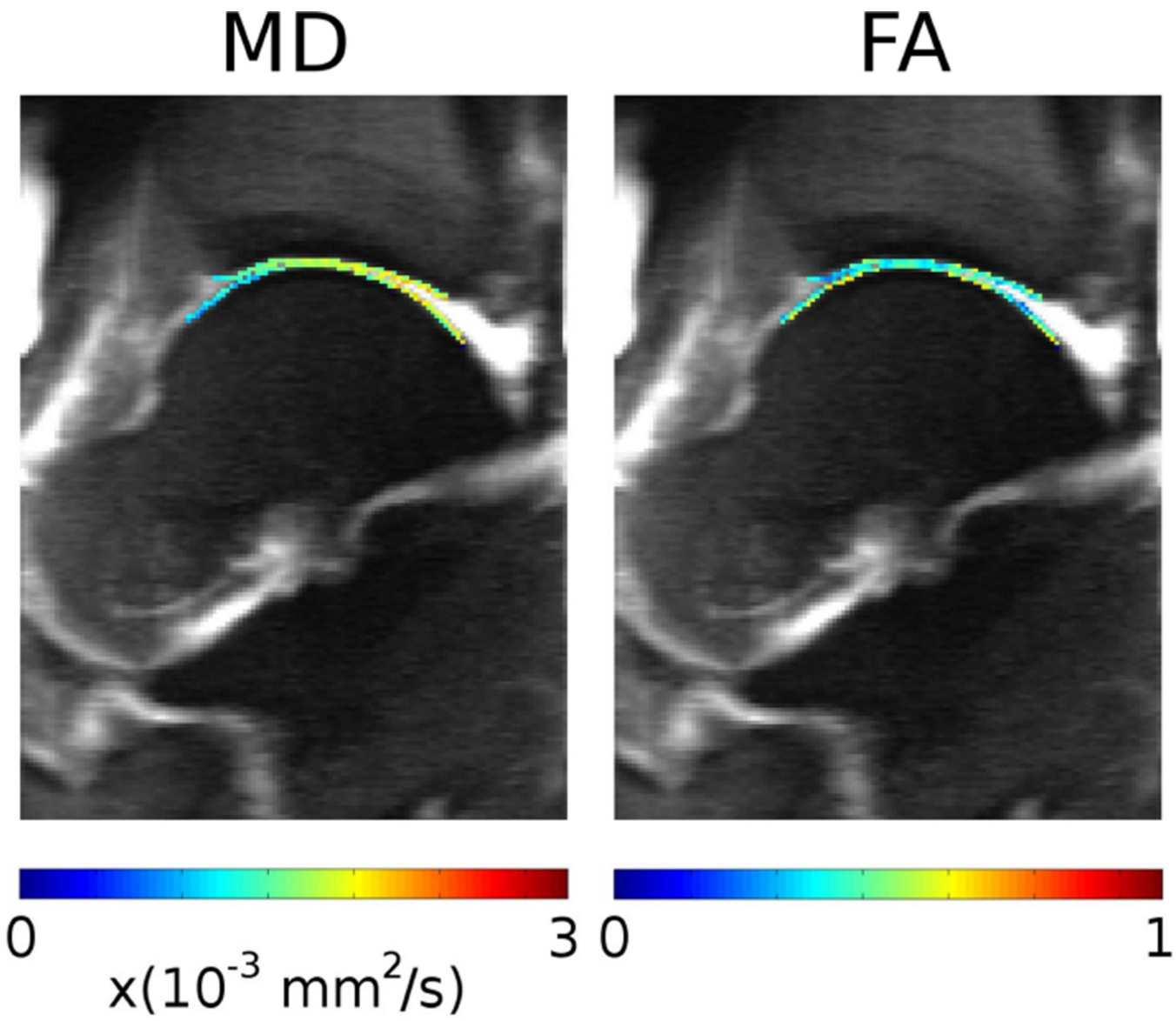

Figure 4.

Line scan diffusion tensor imaging (LSDTI) images of the right ankle of a 28-year-old healthy volunteer acquired at 7T using a custom-built 8 channel carotid coil (TE/TR/TR_{eff}=46/180/2880 ms, matrix=256×128, in-plane resolution=0.5×0.5 mm^2, rotation angle=20°, *b*-values=5,450 mm^2/s, 6 diffusion directions, thickness=3 mm, acquisition time=2:30 min per sagittal slice). The LSDTI is a spin-echo based pulse sequence, where only one line is excited and acquired per repetition time avoiding phase encoding (i.e. motion artifact). Mean diffusivity (MD) and fractional anisotropy (FA) maps of the tibiotalar cartilage are shown in color over the LSDTI b_0-image. Averaged over seven volunteers FA/ADC values were (0.44±0.09) / (1.49±0.18) × 10^3 mm^2/s and (0.48±0.11) / (1.26±0.12) × 10^3 mm^2/s for the tibial and talar cartilage, respectively. *Images courtesy of Dr. Jose Raya, Assistant Professor of Radiology, NYU Langone Medical Center, Department of Radiology*.

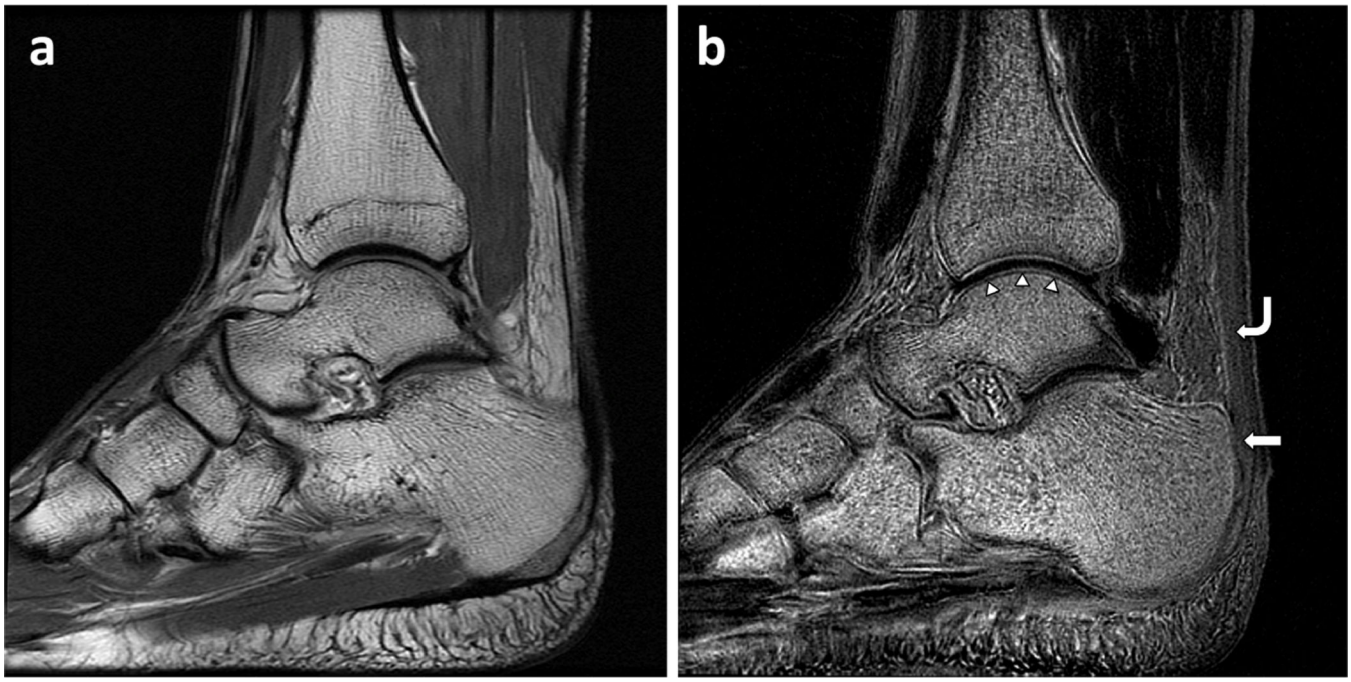

Figure 5.

Comparison of conventional proton density-weighted spin echo image (TE = 19 ms) (**a**) vs. novel ultrashort echo time (UTE) echo subtraction image (TE=0.05 ms minus TE=8 ms) (**b**). UTE image (**b**) shows the deepest layer (including calcified layer) of talar dome cartilage (arrowheads) and the Achilles tensile tendon (curved arrow) and Achilles enthesis (arrow) with high signal intensity. These areas all appear as black signal voids on the conventional proton density-weighted spin echo image (**a**), because of rapid T2 shortening of the tendon and deep layers of hyaline cartilage. These structures have already lost signal by the time they are measured at the conventional echo times and require ultra-short echo time measurement to demonstrate intrasubstance signal.

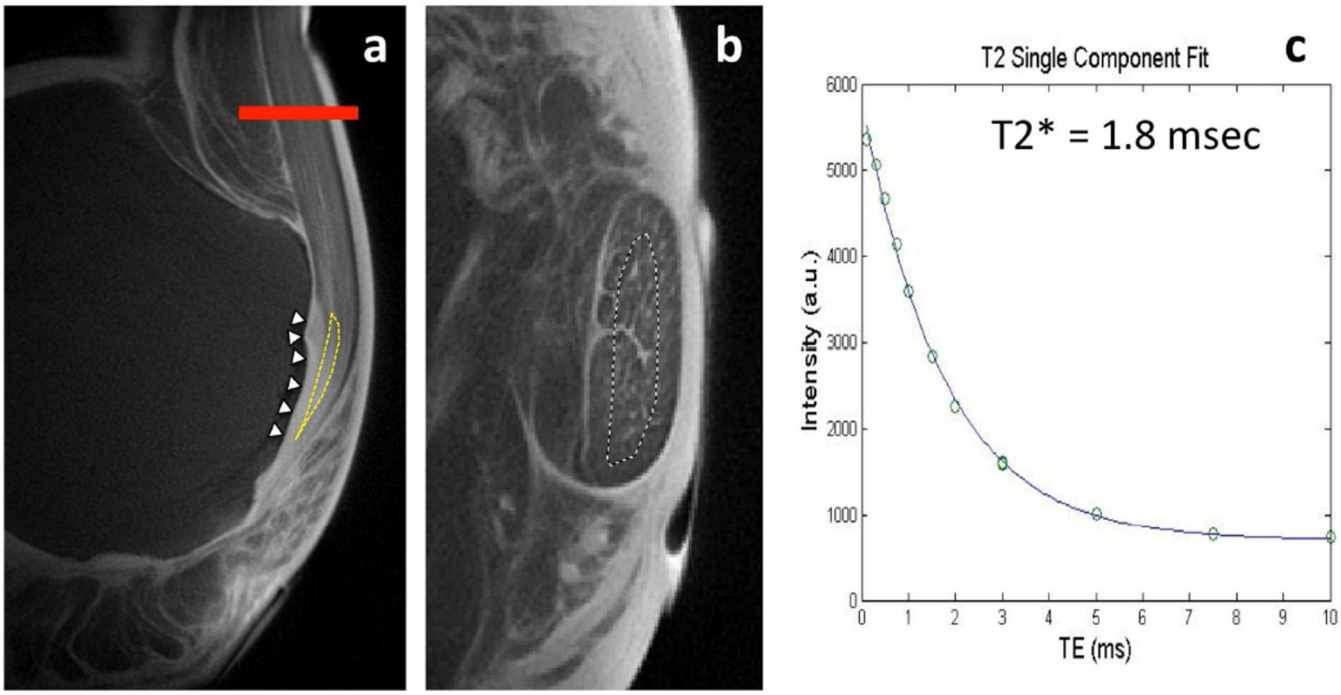

Figure 6.

Sagittal (**a**) and axial (**b**) UTE MR images of Achilles tendon. (**a**) Sagittal image shows fibrocartilage surface of calcaneus (arrowheads) as well as fibrocartilaginous nodule within the tendon (dotted area). In an axial cross section (**a**, thick line; **b**), tensile tendon with normal fascicular appearance can be seen. (**c**) UTE T2* quantification performed on axial images revealed a short T2* value of 1.8 ms, within the normal range.

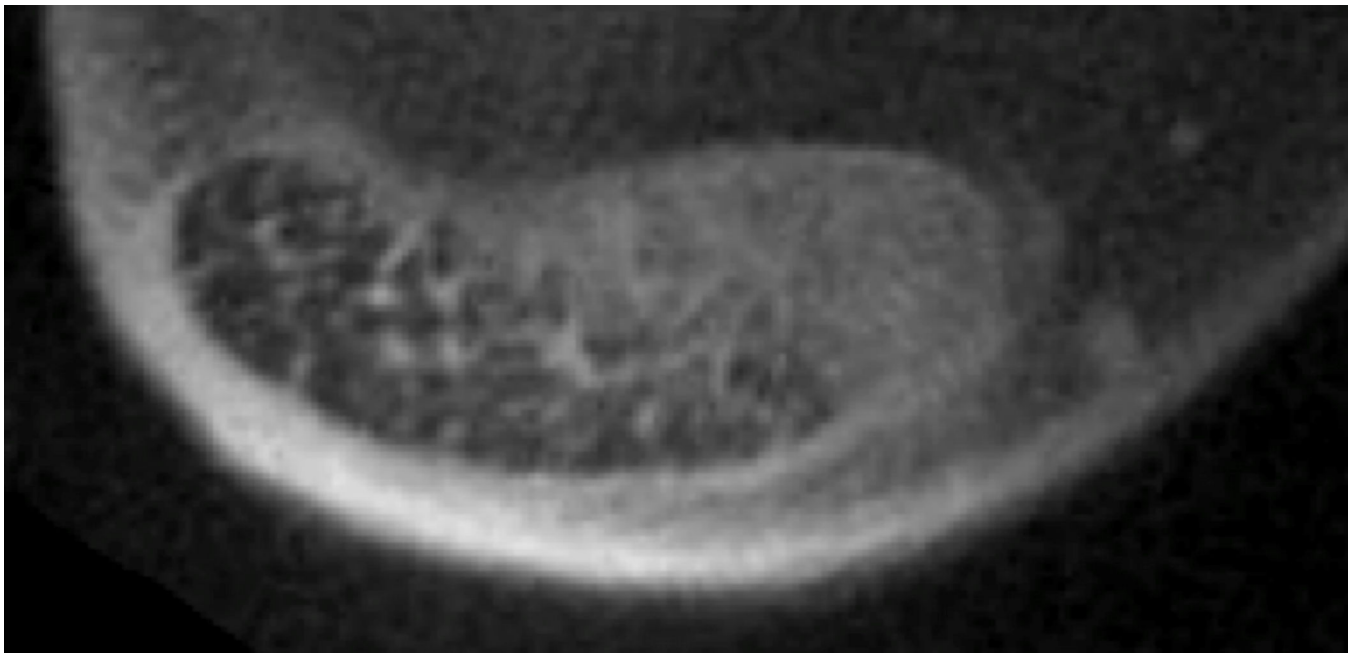

Figure 7.
Axial UTE MR image of Achilles tensile tendon demonstrates differential microstructure of the tendon with geographic effacement of the normal fascicular appearance within the tendon representing intrasubstance degeneration.

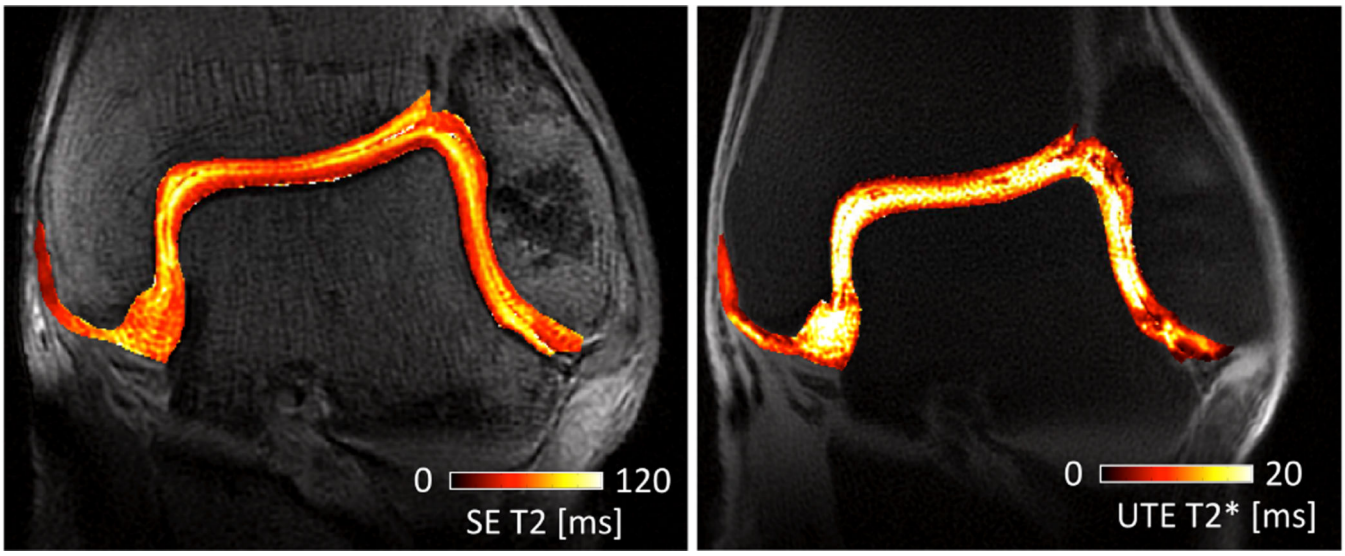

Figure 8.

Color maps of the tibiotalar articular cartilage obtained from conventional multi-echo spin echo T2 (**a**) and ultrashort echo time T2* (**b**) techniques illustrate the short and long T2 components of articular cartilage. T2 (a) map shows the normal zonal variation in T2 values with shorter T2 relaxation times (red band) closer to the subchondral bone, and longer T2 relaxation times (yellow) at the articular surface. In (b) the UTE T2* map, the linear short T2* (red) region adjacent to the subchondral bone interface represents the normal, intact calcified layer of cartilage. The shorter T2* range does not offer evaluation of the integrity of zonal variation in the longer T2 tissue of the more superficial layers of articular cartilage.

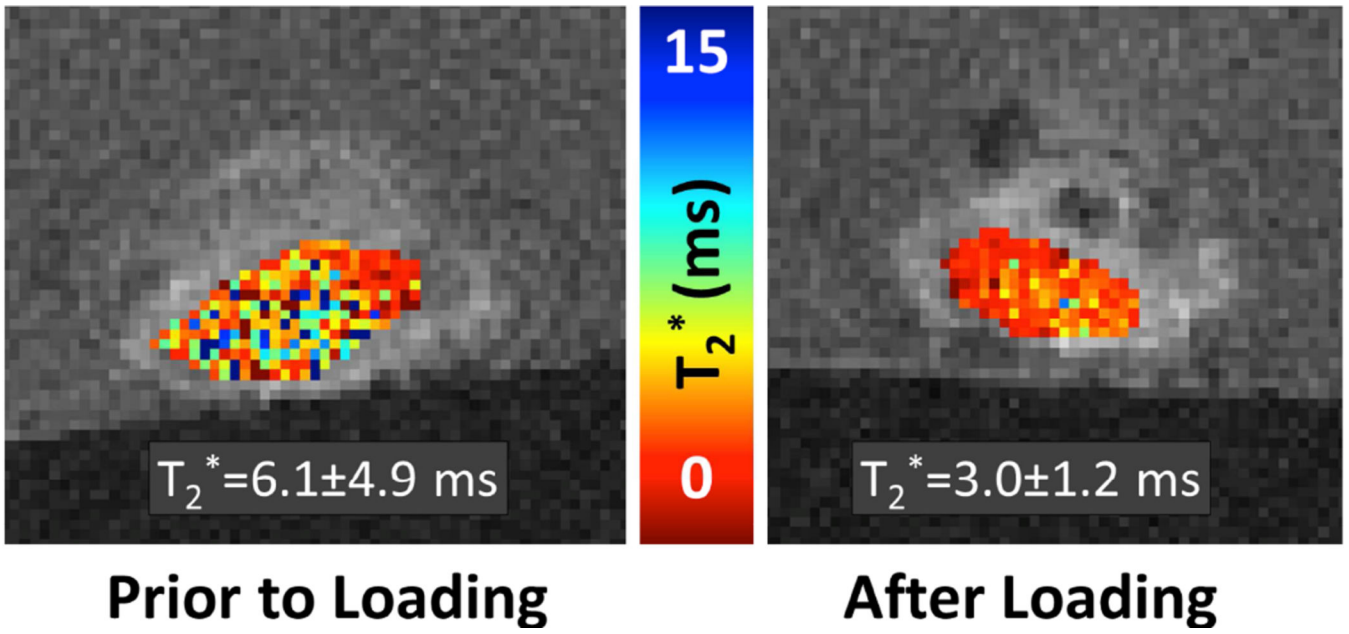

Figure 9.

Tissue evaluation after loading. T2* maps of rabbit patellar tendon before and after 45 Newtons of cyclic loading for 100 cycles. T2* values prior to loading are elevated and have greater variability than corresponding T2* values after loading. Changes in values pre- and post-loading may indicate level of tissue organization and collagen fibril disruption. Evaluation of tissue pre- and post-load may ultimately give insight into tissue function and point of failure. *Images courtesy of Dr. Matthew F. Koff, Associate Scientist, Dr. Hollis Potter, Professor of Radiology, Department of Radiology and Imaging, Hospital for Special Surgery*.

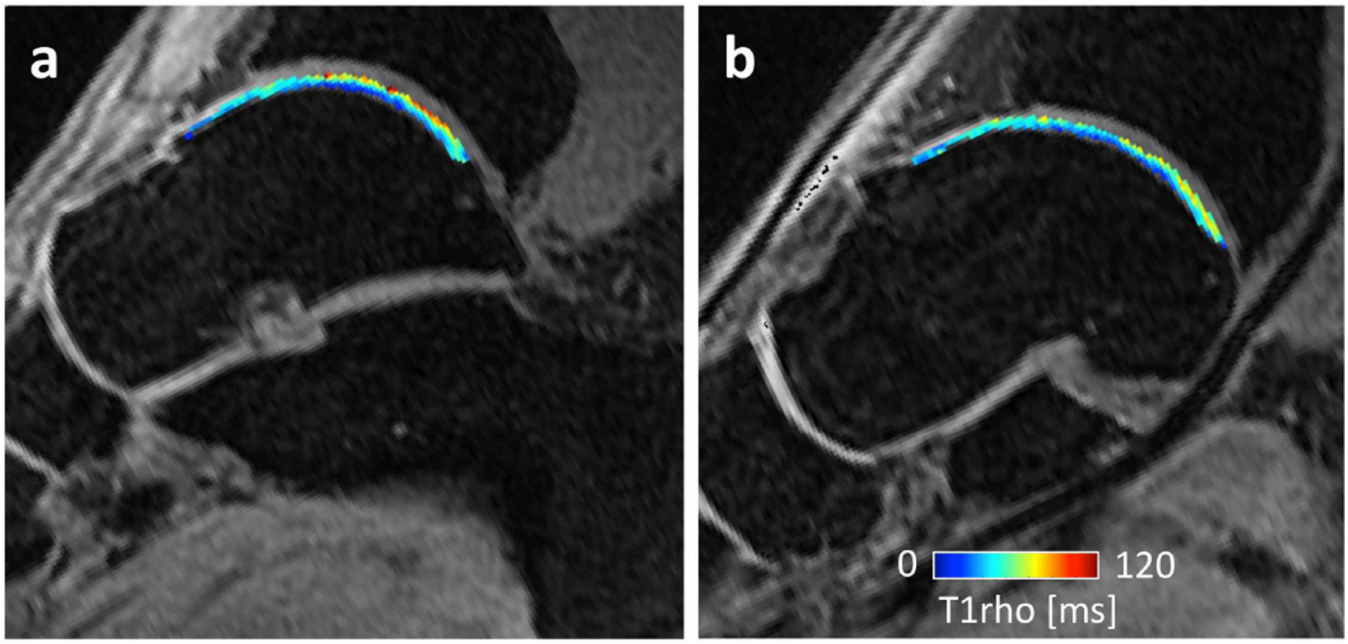

Figure 10.

T1rho mapping of (**a**) lateral and (**b**) medial talar dome cartilage, obtained with the following parameters: TR=8 ms, TE=2 ms, Matrix=256×128, slice=4 mm, spin lock times=0, 10, 40, 80 ms. Some evidence suggests that T1rho mapping reflects proteoglycan content and possibly also collagen fiber orientation and other macromolecules, and that it may be more sensitive than T2 mapping in identifying early hyaline cartilage degradation. *Images courtesy of Dr. Richard Souza, Associate Professor, Department of Physical Therapy and Rehabilitation Science, Department of Radiology and Biomedical Imaging, University of California, San Francisco*.

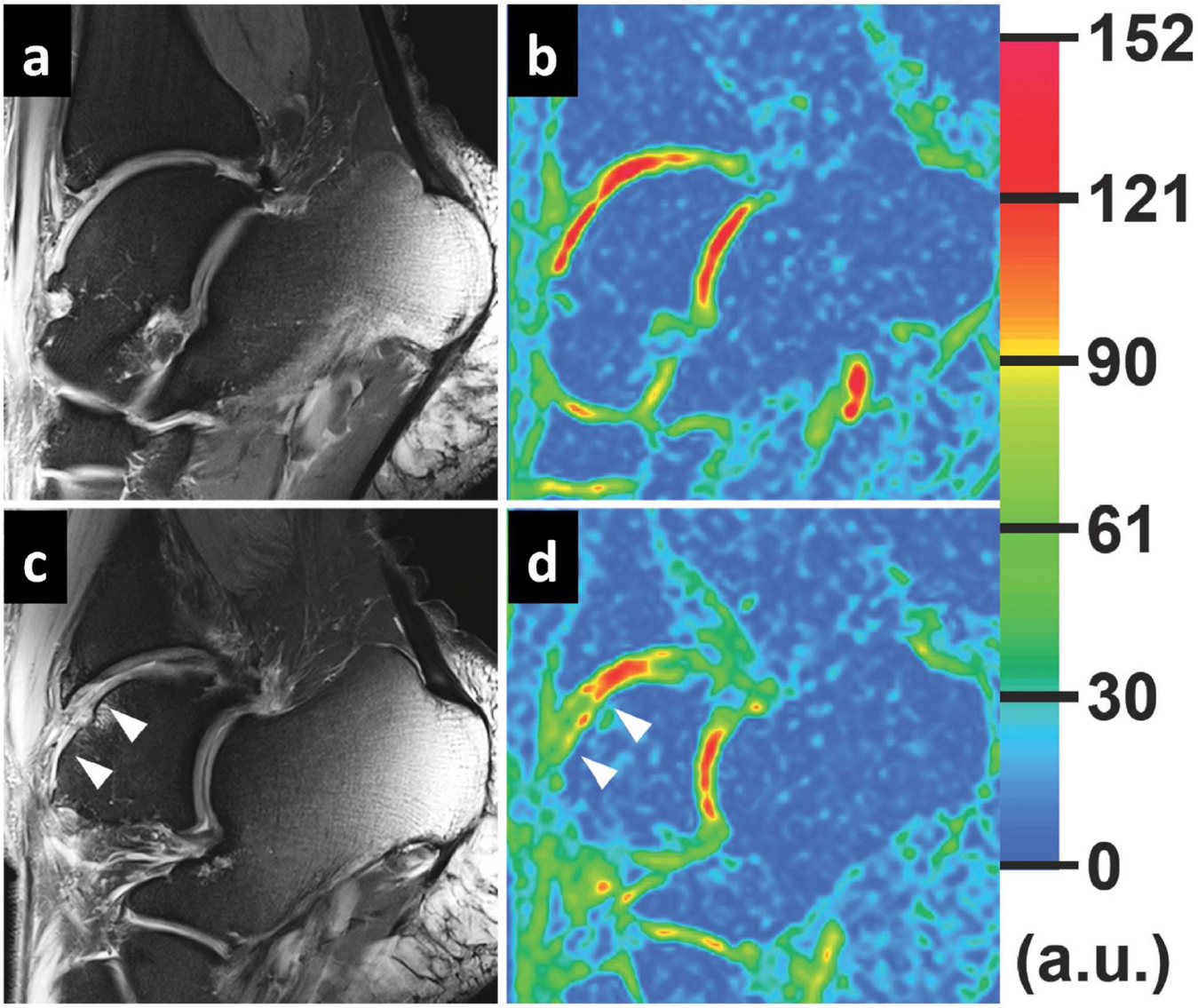

Figure 11.

7 T images of the ankle joint in a 35-year-old male that received microfracture (MFX) treatment 54 months earlier. Images of the medial side (upper row) and of the lateral side (lower row) of the ankle joint. The repair tissue is situated between arrow heads. Proton density-weighted fat-suppressed 2D–TSE images (**a, c**) and corresponding color-coded sodium images (**b, d**) of reference cartilage and repair tissue. *Images courtesy of Dr. Gregory Chang, Associate Professor, Dr. Ravinder Regatte, Professor of Radiology, NYU Langone Medical Center, Department of Radiology*.

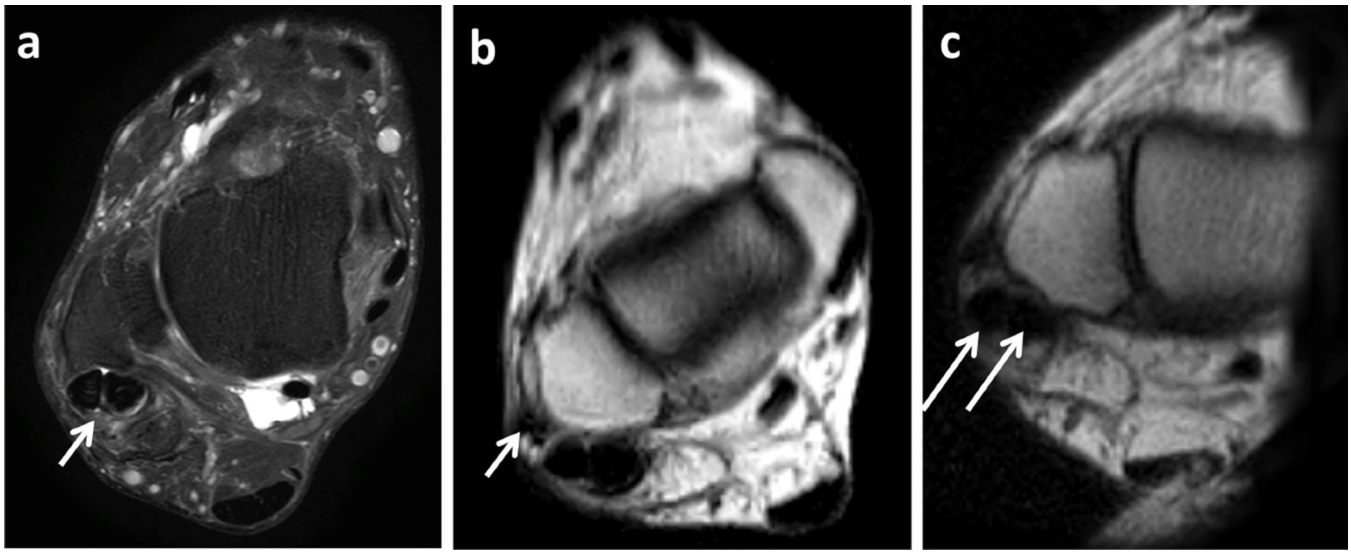

Figure 12.

Kinematic Ankle MRI. Adult male with lateral ankle pain and popping sensation. (**a**) Axial fat-suppressed PD image shows intrasubstance split tears of the peroneal tendons and ill-defined superior peroneal retinaculum (short arrow). (**b, c**) Kinematic MR imaging obtained during real time dorsi- (**b**) and plantar-flexion (**c**) maneuvers show torn and retracted superior peroneal retinaculum (short arrow) and subluxed peroneal tendons on dorsiflexion (long arrows). *Images courtesy of Dr. Vibhor Wadhwa, Radiology intern and Dr. Avneesh Chhabra, Associate Professor Radiology & Orthopedic Surgery, UT Southwestern Medical Center, Dallas, TX*

Table 1

Currently Available and Novel Translational Techniques in MR Imaging of the Ankle and Foot.

MR Techniques	Reference #
Currently Available	
Isotropic 3D FSE for 3D rendering	6–9,18,19
MR neurography	20–22
Diffusion-weighted imaging	20,23,24
Diffusion tensor imaging	31,34,35
Novel Translational	
Ultrashort TE for “invisible” tissues	40–46
Quantitative MR Biomarkers	
○ Collagen-Sensitive	
■ SE T2	60,61,60,64,65
■ UTE T2*	47,72–77,84
○ Proteoglycan-Sensitive	
■ T1rho	85–87
■ Sodium	94–98
Functional Assessment	
○ Kinematic MRI	99–103